Ground Water Monitoring&Remediation

LNAPL in Fine-Grained Soils: Conceptualization of Saturation, Distribution, Recovery, and Their Modeling

by Mark Adamski, Victor Kremesec, Ravi Kolhatkar, Chris Pearson, and Beth Rowan

Abstract

A simple conceptual model is presented that leads to a quantitative description of the behavior of light non–aqueous phase liquid (LNAPL) in fine-grained soil (FGS). The occurrence of large (15 feet) (4.6 m) LNAPL accumulations in observation wells in FGS and of LNAPL located below the water table is explained by macropore theory and capillarity of the FGS. Using soil capillary data, fluid property data, and a simple spreadsheet model, the LNAPL saturation in a soil profile and LNAPL recovery were predicted for a field study site. The predicted LNAPL distribution, saturation, and recovery matched the field observations and actual LNAPL recovery. Measured LNAPL saturations were <2%, while model-predicted values were <3%. The model predicted recovery of ~530 gallons (2009 L). After 1.5 years of continuous operation, a three-phase, high-vacuum extraction system recovered 150 gallons (568 L) of LNAPL. Application of a model that assumes homogeneity of the soil that is heterogeneous at a small scale may seem to be a misapplication; however, conceptualizing the model domain at a sufficiently large scale (3 to 6 feet; 0.9 to 1.8 m) allows for the FGS to be viewed as a homogeneous medium with small effective porosity.

Introduction

Background

The occurrence of light non–aqueous phase liquid (LNAPL) in the subsurface has been the focus of much attention for the past 20 years. Early conceptual models for LNAPL occurrence in the subsurface pictured an LNAPL layer floating on a depressed representation of the capillary fringe or water table (van Dam 1967; Zilliox and Muntzer 1975; Ballestero et al. 1994). This conceptualization was based on experiments in highly uniform sand or glass beads (idealized porous media) because those conditions are easiest to replicate in bench-scale tests and can be performed rapidly. The concept of LNAPL migrating on the capillary fringe, encountering an observation well that has no capillary effect, and the LNAPL draining into the well from the top of the capillary fringe made it possible to explain large (5 or more feet) accumulations of LNAPL in observations wells, while LNAPL recovery attempts in these conditions often resulted in recovery of very little LNAPL. This conceptual model led researchers to develop methods to estimate LNAPL layer thickness in the soil based on thickness observed in the observation wells. Kramer (1982) concluded that the thickness of gasoline measured in a well is roughly two to three times that in the formation. Ballestero et al. (1994) also derived an equation for the formation free-product thickness that is a function of the thickness in the well, the LNAPL specific gravity, and the elevation difference between the LNAPL and the water table.

Two simultaneous papers in 1990, Lenhard and Parker (1990) and Farr et al. (1990), employed capillary pressure and fluid properties to quantitatively describe a different conceptual model for LNAPL occurrence in the subsurface. This conceptual model described a condition where all three phases, air, water, and LNAPL, coexist to varying degrees within a vertical zone in the soil profile that is loosely constrained by the elevation of the water table. What is important about these papers is that they explained that LNAPL is not present in a single uniform layer of high LNAPL saturation on the water table. Both papers stated in essence that "oil-saturated 'pancakes' do not develop in the vast majority of soils and aquifers" (Lenhard and Parker 1990). Huntley et al. (1994) provide data showing a good comparison between the predictions resulting from the Lenhard and Parker model and field observations.

The aforementioned work was developed for and applied to primarily coarse-grained porous media, such as sands and gravels. Little research has been done to evaluate the applicability of the theories to describing LNAPL

Published in 2005 by the National Ground Water Association.

behavior in fine-grained soil (FGS). The research conducted to date has investigated dense non–aqueous phase liquid (DNAPL) occurrence in "fractured" FGS (Kueper and McWhorter 1991; Parker et al. 1994; Hinsby et al. 1996; Freeze and McWhorter 1997; O'Hara et al. 2000). Very little work on the behavior of LNAPL in FGS is available. Some of the concepts that describe DNAPL behavior in FGS are applicable to LNAPL, such as threshold entry pressure, while others such as depth of non–aqueous phase liquid (NAPL) penetration are not. This paper focuses on sites that consist of FGS throughout the region of LNAPL presence.

Using mathematical relationships to describe LNAPL saturations in the interval of LNAPL impact similar to those developed by Lenhard and Parker (1990) and Farr et al. (1990), Charbeneau and Chiang (1995) developed a simple model for predicting LNAPL recovery. Charbeneau et al. (1999) in the American Petroleum Institute (API) report extended these models and incorporated them into a spreadsheet and report for evaluating the recoverability of LNAPL from the subsurface. These spreadsheet models are available from the API at www.api-ep.api.org/environment from the Light Non-Aqueous Phase Liquid (LNAPL) Resource Center. This API report incorporated the advancements in understanding LNAPL occurrence that were made in the previous decade.

Several field observations such as LNAPL detected 15 or more feet (4.60 m) below the water table when historic water level fluctuation cannot explain such an occurrence; very small volumes of LNAPL observed in the surrounding soil when the observation well contains many feet of LNAPL; very low LNAPL recovery volumes when large LNAPL accumulations are present in neighboring wells; apparent LNAPL migration below the water table; and rapid water level response, associated with rainfall events, in observation wells screened well below the surface led to an interest in the topic of LNAPL occurrence and migration in FGS. Because these observations did not fit with the understanding of LNAPL in idealized porous media (glass beads), the authors felt the need to develop and extend the model of Lenhard and Parker (1990) and Farr et al. (1990) to describe LNAPL migration in FGS.

The objectives of this paper are to (1) develop a conceptual model for LNAPL migration in FGS that extends the concepts developed in research on DNAPL migration in FGS and the LNAPL work of Lenhard and Parker (1990) and Farr et al. (1990), thereby providing a sound explanation for the aforementioned LNAPL field observations; (2) evaluate the applicability of the Charbeneau/API model (Charbeneau et al. 1999) for predicting LNAPL recovery in FGS; and (3) compare the predictions of LNAPL saturation and recovery from the Charbeneau/API model with the actual saturation and recovery of LNAPL at one FGS field site.

Development of the Conceptual Model for LNAPL in FGS

Structure of FGS

Before presenting a conceptual model for the behavior, movement, and saturation of LNAPL in FGS, an understanding of the hydrogeology, hydraulics, and physical structure of the air/water/FGS system must be developed. FGS has often been described as possessing dual porosity or as being fractured (Kueper and McWhorter 1991; Parker et al. 1994; Hinsby et al. 1996; Freeze and McWhorter 1997; O'Hara et al. 2000). Much of this cited work in FGS focused on fractured FGS containing DNAPL. These authors conceptualized the pores that control DNAPL migration as fractures, although Hinsby et al. (1996) discussed root holes in addition to fractures. Corey (1986) envisioned FGS as having a "very wide pore-size distribution," thus treating the soil as a whole with pores ranging in size from very small to very large. In contrast to FGS, highly uniform coarse sand can be described as having a very narrow distribution of pore sizes, all being relatively large. In this paper, the term "fracture" will not be used to describe the large pores in FGS due to the semiplanar geometry that is implied by the term. The term "macropore" will instead be used to describe the larger pores that constitute the high end of the FGS pore size distribution. Brockman and Szabo (2000) provide an example study into the mechanics and formation of structure and macropores in FGS.

FGS tends to be highly structured, which means it contains matrix blocks. Matrix blocks are areas in the FGS generally devoid of macropores, or at least any interconnected macropores. There are also areas in FGS that contain macropores. Figure 1 shows an FGS with stained macropores. This picture serves as an excellent example of a typical FGS containing matrix blocks and macropores. Figure 2 is a picture of highly plastic clay (Unified Soil Classification

Figure 1. Photo showing stained macropore network in doleritic clay. Note: vertical white bar is a meter stick for scale.

Figure 2. Photo of highly plastic clay (CH). When sample was cut, LNAPL bubbled out of macropores and created the hydrocarbon sheen halo around macropores that can be seen around the six macropores. Note: this soil is behaving as a water-wet soil would be expected.

System, USCS, classification CH) showing six macropores filled with LNAPL. When the core in Figure 2 was cut, exposing the LNAPL-filled macropores, the LNAPL bubbled to the surface of the core, leaving the hydrocarbon halo (sheen) that is visible around the six macropores.

Macropores are generally very small structures (<1 mm) that are large enough to exhibit low capillary entry pressures. It will be shown, with respect to LNAPL and to a large degree the same is true of water migration, that macropores in FGS are equivalent to and constitute the effective porosity. Domenico and Schwartz (1990) and Bear (1972) discuss the effective porosity in FGS and suggest that the effective porosity of FGS is "much smaller than" total porosity. The definition of macropore is intended to include any large pore in FGS. An FGS, such as a lacustrine clay or a deep water tertiary sediment, is likely not structured, but neither of these soils is relevant to the majority of shallow subsurface LNAPL sites.

Vertical Gradients in FGS

Large vertical gradients are commonly observed in FGS. Simpkins and Bradbury (1992) found that vertical gradients in Wisconsin glacial till ranged from 0.11 to 0.76 at five sites with an average of 0.39. Hinsby et al. (1996) described vertical gradients of 0.45 as being typical in till deposits in Denmark. In reviewing sites for this study, similarly high vertical gradients were found at FGS sites in the Midwestern, Gulf Coast, and Southeastern portions of the United States (Table 1. Saturated FGS tends to have vertical gradients that are one to two orders of magnitude greater than the horizontal gradient (see Table 1 for additional information). Therefore, water moves vertically rather than horizontally in FGS. These large vertical gradients are the result of precipitation percolating through the surficial FGS and recharging to an underlying permeable zone that allows lateral migration of the water (see Domenico and Schwartz 1990, figure 7.11b, or Freeze and Witherspoon 1967, for further discussion).

Moisture Conditions in Surficial FGS

The matrix blocks of a structured FGS are likely to be highly water saturated because in a dry state the capillary pressure is so high that infiltrating water and/or saturated zone water would be drawn into the small matrix pores. The existence of high saturation can be shown by evaluating the potential for capillary rise from the water table. McWhorter (1995) calculated the height of capillary rise for the matrix blocks in an FGS with a hydraulic conductivity of 1×10^{-6} cm/s to be 16.7 feet (5.1 m). Grain size data collected from the Midwestern U.S. site associated with this study resulted in estimates for the height of capillary rise to be 25 feet (7.8 m), using the method of Jury et al. (1991). For larger pores, McWhorter (1995) calculated the height of capillary rise in a fracture, with a 0.1-mm aperture, to be 4.7 inches (0.12 m). Similarly, using another equation to calculate capillary rise (Jury et al. 1991), one can calculate the height of capillary rise in a 0.5-mm-diameter macropore to be only 2.2 inches (0.056 m). At these sites, the depth to ground water ranges from 7 to 14 feet (2.1 to 4.3 m) below ground surface (bgs). This shallow water level would result in the matrix blocks being nearly water saturated between the water table and the ground surface, while the macropores would be dry. In fact, at the Midwestern site, saturations ranging from 90% to 94% were measured in the vadose zone (PTS Laboratories 2000, 2002). It is proposed here that during precipitation events, water that is percolating through the macropores will move past the matrix blocks and be subject to the high capillary pressures of any dry portions of the matrix blocks, thus being drawn into and saturating the FGS matrix, with any excess water rapidly migrating down through the macropore network.

Vertical Connectivity and Depth of Macropores

Although macropores may be a surficial feature resulting from shrinkage of the FGS or shallow root structures,

Table 1
Observed Hydraulic Gradients at the Three Study Sites

Site	Stratigraphic Section of Gradient	Vertical Gradient (–) = ratio	Horizontal Gradient (–) = ratio
Gulf Coast	FGS to underlying permeable unit	0.10	0.002
Midwestern	FGS to base of FGS	0.10 to 0.30	0.08
Southeastern	Within FGS	0.22 to 0.33	0.01
Southeastern	FGS to base of FGS	0.50 to 0.70	0.01
Southeastern	FGS to underlying limestone	0.43 to 0.52	0.01

Simpkins and Bradbury (1992) documented macropores as deep as 33 feet (10 m) and stated "hydraulic conductivity, hydraulic head, and geochemical data suggest their effectiveness is greatest to a depth of about 10 m." The studies listed earlier on DNAPL migration in macropores indicate that it has been found necessary to evaluate NAPL migration in such features.

Figure 3 is a graph of water level elevation and daily precipitation as a function of time for a representative well at the Southeastern U.S. FGS site. The top of the well screen for the well depicted in Figure 3 is located 12 feet (3.65 m) bgs. Data in Figure 3 indicate that the percolating precipitation begins to impact the water level in the well almost instantaneously and has completed percolation within 3 to 5 d. Thus, given the rapid response of the water levels in observation wells to precipitation events at this site, it is very likely that the macropore network is well connected in a vertical sense. Downward vertical gradients in FGS at this site result from infiltrating water migrating into underlying horizontal permeable zones. Large vertical gradients in FGS at this site are associated with periods of precipitation, while lesser vertical gradients are associated with periods lacking precipitation.

Using Darcy's law and hydraulic conductivities ranging from 1.6×10^{-8} to 50×10^{-8} cm/s and vertical gradients ranging from 0.11 to 0.76 for Wisconsin glacial tills, Simpkins and Bradbury (1992) estimated the vertical seepage velocity above the water table to range from 0.4 to 20 cm/yr. Using the following data from the site portrayed in Figure 3, vertical hydraulic conductivity equal to1.6×10^{-7} cm/s (lab measured from a 3-inch [7.5-cm] undisturbed core); a conservative vertical gradient of 1 (site value is typically 0.22 to 0.33); effective porosity of 0.05 (estimated based on storativity values from similar soils), and the same method used by Simpkins and Bradbury, the rate of rain water percolation should be ~3.2 ft/yr (1 m/yr) or more than 3 years to percolate 12 feet (3.65 m). Using a different method, Stephens (1996) explains that the velocity of a percolating wetting front in the vadose zone is approximately equal to the hydraulic conductivity divided by the change in moisture content (moisture content behind the wetting front minus the initial moisture content). The moisture content of the soils below the water table at the site depicted in Figure 3 is ~0.36, and assuming an initial moisture content ranging from 0.28 to 0.33, the estimated wetting front velocity would range from 2 to 5 ft/yr (0.6 to 1.5 m/yr).

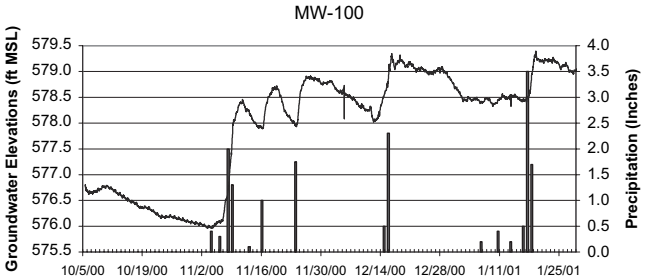

Figure 3. Water level (line graph) and daily rainfall (bars) in a typical monitoring well at an FGS site (width of vertical bar is 1 d). Note: Top of well screen is 12 feet bgs.

However, the water level responses shown in Figure 3 illustrate that the precipitation is finding a much more efficient pathway for downward migration than migrating through the primary porosity of the FGS. As a result, it is hypothesized that the macropore network is effective down to 12 feet (3.65 m), the depth that corresponds to the top of the screened interval in the well. These findings are consistent with those of Hinsby et al. (1996). In their work, Hinsby et al. (1996) measured vertical migration rates of 4 to 360 m/d through macropores in the FGS.

It should be mentioned that other research suggests that such a water level response could theoretically be the result of an air pressure wave leading the infiltrating wetting front that results from precipitation events (Bianchi and Haskell 1966; McWhorter 1971). However, the results of those studies were based on changes in soil water content (Bianchi and Haskell 1966) and laboratory cell experiments and numerical model results (McWhorter 1971) rather than on actual water particle tracer testing. In spite of the measurement technique, Bianchi and Haskell observed the soil "wetting front" to penetrate to a depth of 10 feet (3 m) in a clay loam soil in 10 d, much faster than the aforementioned two methods would have predicted. Thus, the observations made at the site depicted in Figure 3, the work of Bianchi, and the work of Hinsby et al. (1996) justify the position of this paper that the water level changes observed in Figure 3 are the result of water migrating through the macropores in the FGS and collecting in the observation well. This is evidence for effective macropore networks to a depth of at least 12 feet (3.65 m) bgs.

In summary, FGS consists of matrix blocks and macropores. The macropores can be well interconnected, comprise a very small fraction of the total soil volume, and possess little capillary pressure when compared to adjacent matrix blocks. The majority of the FGS volume is composed of matrix blocks that maintain very large capillary pressure, so the water contained in those blocks is held very tightly.

Hydraulics of LNAPL in FGS

The capillary pressure that must be overcome by a nonwetting LNAPL to enter a water-saturated pore, the threshold entry pressure, is defined by the following relationship (Mercer and Cohen 1990):

$$h_c = \frac{(2\sigma \cos\phi)}{(r\rho_w g)} \quad (1)$$

where r is the radius of the water-filled pore, ρ_w is the density of water, g is the gravitational constant, σ is the interfacial tension between the LNAPL and the wetting fluid, and ϕ is the contact angle measured into the water, in degrees.

For example, using the soil particle size analysis data from the Southeastern FGS site (sandy lean clay, CL) to approximate the size of an average pore radius of the soil matrix (D_{10} and 1/5 D_{10}; 0.005 and 0.001 mm, respectively) (Bear 1972), the LNAPL/water interfacial tension of 20.6 dyne/cm and LNAPL specific gravity of 0.86 measured (PTS Laboratories, Santa Fe Springs, California) from site fluids (weathered *m*, *o*, and *p*-xylene and ground water), and a literature-based contact angle of 40°, the required threshold entry pressure for the LNAPL to enter

into water-saturated pores ranges from 4.2 to 21 feet (1.28 to 6.4 m) of water or 4.9 to 24 feet (1.5 to 7.3 m) of LNAPL. Thus, for LNAPL to enter the pores in the soil matrix, the LNAPL must develop a pressure equal to an LNAPL pool 4.9 to 24 feet (1.5 to 7.3 m) deep. In contrast, the threshold entry pressure for LNAPL to enter a water-saturated, 0.5-mm-diameter macropore is only 0.59 inch (1.5 cm) of LNAPL. These calculations assume that the soil is water saturated. In true field conditions, such a macropore at the ground surface would likely be dry and thus have no threshold entry pressure for the LNAPL to overcome. Kueper and McWhorter (1991) developed a very similar rationale, with similar findings, to demonstrate the significance of entry pressure and macropores in the migration of DNAPL. The importance of the macropore for fluid migration within FGS is the result of the low permeability and the high capillary entry pressure (threshold entry pressure) of the matrix blocks of the FGS. Therefore, it is not surprising that macropores could act as the preferential pathway for LNAPL migration in FGS.

Figure 4 depicts a hypothetical spill of LNAPL into an FGS. Other spill scenarios, such as leaky underground lines, can also result in similar conditions. In this scenario, a release of diesel fuel into a diked area creates a puddle of LNAPL (Z_p) 6 inches (15.2 cm) deep above the FGS ground surface. The macropore depicted has a diameter of 0.5 mm, the LNAPL has a density of 0.86 g/cm^3, the interfacial tension for the LNAPL/ground water is 20.6 dyne/cm, the contact angle is 40°, and the depth to ground water (Z_w) is 2 feet (0.6 m). Given this information and assuming hydrostatic equilibrium, and setting the threshold entry pressure equal to zero for the macropore and assuming the parameters mentioned subsequently, the depth of LNAPL penetration below the water table (Z) is 15.4 feet (4.7 m). Taking the threshold entry pressure into account, the equation for depth of LNAPL penetration below the water table (Z) can be calculated using Equation 2.

$$Z = \frac{(Z_w + Z_p)\rho_{\text{oil}} - h_c \cdot \rho_{\text{w}}}{(\rho_{\text{w}} - \rho_{\text{oil}})} \qquad (2)$$

where $h_c = 2\sigma_{ow}\cos\theta/r\rho_w g$, Z_w = depth to water table, Z_p = depth of LNAPL pool on surface, σ_{ow} = interfacial surface tension, θ = contact angle, ρ_w = density of water = 1 g/cm^3, ρ_{oil} = density of LNAPL, h_c = threshold entry head for LNAPL into water wet pore derived from Equation 1.

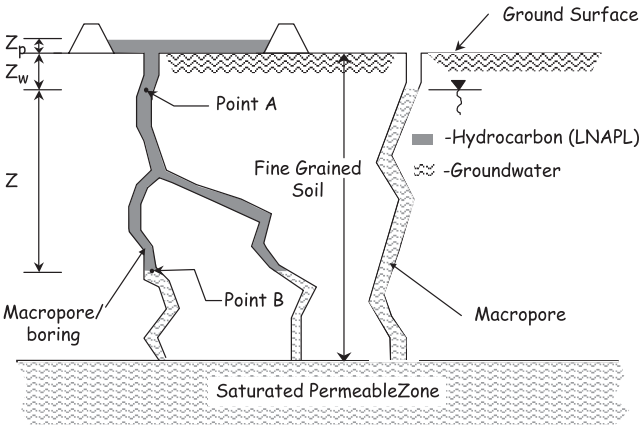

Figure 4. Conceptual model for LNAPL infiltration into a macropore network in FGS.

Assuming the same parameters and using Equation 1 to calculate the threshold entry pressure for LNAPL into the 0.5-mm macropore, the depth of LNAPL penetration calculated using Equation 2 is 15.1 feet (4.6 m) below the water table.

The aforementioned process of LNAPL buoyancy and penetration is analogous to that of an iceberg where the LNAPL is confined laterally within the macropore and the LNAPL in the LNAPL-saturated pore above the water table acts as the tip of the iceberg. With this LNAPL "iceberg" effect, it is understandable how LNAPL can be pushed several feet below the water table through macropores in FGS. In this specific example (Figure 4), 2.5 feet (0.76 m) of excess hydrocarbon head was developed based on pool depth and thickness of the unsaturated zone. As the thickness of the unsaturated zone varies so to will the depth of LNAPL penetration. LNAPL migrates down through the macropore network in FGS, filling any horizontal pores with sufficiently low threshold entry pressure until the LNAPL reaches hydraulic equilibrium with the ground water in the macropores or until a laterally extensive permeable layer (such as a sand layer) is encountered. If this permeable layer is encountered, the LNAPL can migrate into the sand and relieve the excess LNAPL pressure that is developed from the spill in the unsaturated zone. If extensive horizontal migration is possible so that the LNAPL is not confined to macropores due to a low threshold entry pressure, then it is expected that the penetration of LNAPL below the water table will be much less than calculated earlier. This iceberg effect will only hold true as long as the LNAPL is restricted to macropores and cannot migrate laterally.

The aforementioned example and Equation 2 do not account for a condition with a vertical hydraulic gradient. The impact of vertical hydraulic gradients on LNAPL migration in FGS must be considered because vertical gradients in FGS are common (Table 1). Mercer and Cohen (1990) describe the minimum vertical hydraulic gradient required to prevent upward LNAPL movement (floating to the top of the fluid column) using the following relationship:

$$\frac{\Delta h}{\Delta z_{\text{oil}}} = \frac{(\rho_{\text{oil}} - \rho_{\text{w}})}{\rho_{\text{w}}} \qquad (3)$$

where Δh is the head difference across an LNAPL ganglion (units L), Δz_{oil} is the elevation difference of the top and bottom of the LNAPL ganglion (units L), ρ_{oil} is the LNAPL density, and ρ_w is the density of water. Equation 3 neglects capillary pressure, which has already been shown to be negligible in the macropores of FGS. Using the same LNAPL (diesel fuel) (ρ_n = 0.86) as an example, the minimum vertical gradient needed to prevent upward LNAPL migration is 0.14. Comparing this result with the vertical gradients in Table 1, it is evident that LNAPL can also migrate downward in FGS as a result of the high vertical gradients that are encountered in such soils. Thus, LNAPL can penetrate below the water table as a result of either of the two conditions, hydrostatic pressure or vertical hydraulic gradient, or some combination of the two conditions.

Equation 4 is the general equation for calculating the depth of LNAPL migration below the water table that accounts for both aforementioned conditions, including threshold entry pressure. Figure 4 can also be used to depict a condition with an LNAPL head of $Z_w + Z_p$ above the water table in the presence of a downward vertical hydraulic gradient (J_z). In this hypothetical case, LNAPL has entered the macropore system and migrated downward to a depth, Z, below the water table. At point B, which is located at this depth Z, the pressure of water and LNAPL is the same. The LNAPL pressure is calculated using hydrostatics, while the water pressure must consider the downward movement of percolating water under a hydraulic gradient J_z (downward gradient is positive). Equating the pressures at point B gives the following relationship:

$$Z = \frac{\rho_{oil}(Z_w + Z_p) - \rho_w h_c}{\rho_w(1 - J_z) - \rho_{oil}} \quad (4)$$

Equation 4 demonstrates that if $J_z \geq 1 - \rho_{oil}$, then the hydraulic gradient will carry the LNAPL down to the underlying permeable zone where the vertical hydraulic gradient would be dissipated. Likewise, an upward gradient will limit the depth that the LNAPL will penetrate below the water table. Equation 4 is only applicable when $J_z < 1 - \rho_{oil}$.

LNAPL Accumulation in Observation Wells

Figure 5 is a schematic of what happens when excess LNAPL pressure, or gradient, is sufficient to permit LNAPL entry into a permeable zone that is below the water table. If a monitoring well is screened in the permeable zone that contains LNAPL, the well will fill with LNAPL from that permeable zone. "Bottom-up" filling may also occur when observation wells screened in FGS intersect macropores that are filled with LNAPL that is located below the water table.

Large LNAPL accumulations in observation wells in FGS are not the result of LNAPL floating on top of the capillary fringe in FGS, as was described in the now-discredited models of van Dam (1967) and other authors. Rather, they are the result of LNAPL that is confined to the macropore network below the water table that drains into wells. Given enough time, due to the low LNAPL flux from these pores and sufficient LNAPL volume in the macropore network, the LNAPL thickness in the well will extend from slightly above the water table, resulting from the fluid density difference, down to the deeper macropores containing LNAPL. The equations for determining the precise elevations of these LNAPL/air and LNAPL/water interfaces are presented in Lenhard and Parker (1990) and Charbeneau et al. (1999).

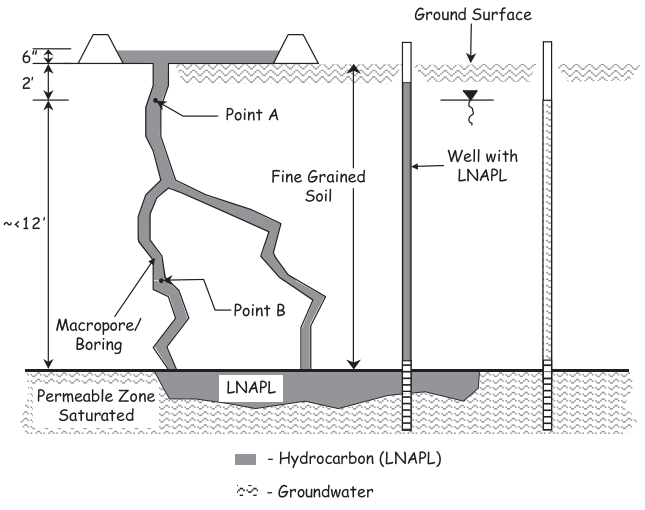

Figure 5. Schematic depiction of LNAPL bottom-up filling of a monitoring well, resulting in exaggerated LNAPL accumulation.

Proposed Conceptual Model

From the aforementioned observations and calculations, the following conceptual model for LNAPL behavior in FGS is proposed. FGS is structured, and the structure consists of matrix blocks and macropores. Macropores have a low threshold entry pressure compared to pores in the matrix blocks and thus the LNAPL enters and is confined to only the macropores in the FGS. The hydraulic gradient in FGS has a very large vertical component that is commonly two orders of magnitude greater than the horizontal component. LNAPL spills result in hydrocarbon entering the macropores above the water table; these LNAPL-saturated macropores then result in excess LNAPL pressure (in excess of hydrostatic) at and below the water table. As a result of the LNAPL being confined to the macropores, the large vertical hydraulic gradients, and the excess LNAPL pressure, LNAPL can penetrate below the water table through macropores, leading to the following troublesome field observations: (1) large (15+ feet) (4.6 m) accumulations of LNAPL in wells, yet (2) LNAPL occupying very small portions of the pore space (<5%) and resulting in low volumes of recoverable LNAPL.

Application of the API/Charbeneau Model to an FGS

Charbeneau et al. (1999) developed the model used to predict LNAPL distribution and recovery in this work. This formulation uses the Brooks and Corey (1964) or van Genuchten (1980) model for capillary pressure/soil moisture retention data to predict the LNAPL distribution in soil, and the Charbeneau and Chiang (1995) hydraulic recovery model as the basis for recovery predictions. The model uses spreadsheets that are intended to be tools for using site-specific data to evaluate the distribution and recovery of LNAPL from porous media near the water table in unconfined ground water conditions. This version of the API/Charbeneau model consists of two spreadsheets. The first spreadsheet calculates the LNAPL saturation and distribution in the soil profile based on LNAPL pressure and soil capillary data. The second spreadsheet uses output from the first to estimate the recovery of LNAPL as a function of the recovery of another fluid, either air or water.

The significant assumptions required by both the distribution and recovery models are homogeneity of the porous

medium, vertical equilibrium of the LNAPL/ground water system, and unconfined/water table ground water conditions. Output of the model includes information such as the LNAPL saturation profile, LNAPL specific volume (D_o) (L^3/L^2) for a given thickness of LNAPL in a well, and recovery volumes as a function of time for a given recovery scenario. D_o, the LNAPL specific volume, is the integral of the LNAPL volumetric content (saturation multiplied by porosity) over the entire depth of the soil column and should not be confused with or conceptualized as a continuous layer of LNAPL in the soil formation. Instead, it represents the combined thickness of LNAPL that would result if the soil and water are removed from the entire LNAPL-impacted soil column and the disseminated LNAPL was allowed to coalesce. To estimate LNAPL recovery, both the LNAPL specific volume (D_o) and the LNAPL relative permeability may be represented as piece-wise linear functions of LNAPL thickness in a well. Charbeneau et al. (1999) and Charbeneau (2003) describes how these representations allow development of relatively simple models for predicting the performance of free-product recovery systems. For example, Equation 5 is used to estimate LNAPL recovery (Q_o).

$$Q_o = \frac{\rho_o \mu_w \bar{k}_{ro} Q_w b_o}{\rho_w \mu_o b_w} \equiv \frac{\rho_r \bar{k}_{ro} Q_w b_o}{\mu_r b_w} \quad (5)$$

where Q_o is the discharge rate of the LNAPL, Q_w is the discharge rate of water from the recovery system, μ_w and μ_o are the viscosities of the water and LNAPL, respectively, k_{ro} is the relative permeability of the LNAPL, b_o is the LNAPL thickness in the well, and b_w is the effective thickness of the aquifer.

LNAPL Distribution Modeling

The van Genuchten model parameters were used in the Charbeneau formulation to predict the LNAPL saturation distribution in the FGS. A benefit of the van Genuchten model is that it predicts there is essentially no threshold capillary entry pressure; that is, LNAPL can enter the soil at essentially zero capillary pressure, which is consistent with the macropore theory discussed earlier. Thus, very low saturations of LNAPL will be predicted to occur in the soil, and since large capillary pressures are required to displace water from the fine-grain matrix blocks, these low saturations will be the maximum typically observed in the field. This prediction confirms the authors' experience with FGS sites. The low LNAPL saturations will be demonstrated in the example site that is described subsequently.

Field Study Site

Hydrogeology

The site used in this application of the API/Charbeneau model is an FGS site located in the Midwestern United States. The soil strata at the study location can be described as 27 feet (8.3 m) of clay overlying impermeable bedrock with ~1 feet (0.3 m) of weathered bedrock from 27 to 28 feet (8.3 to 8.4 m) bgs. The fines content within the clay ranges from 85% to 95%, with the remaining coarse fraction being fine sand. Macropores containing LNAPL have been observed in the FGS at this location during soil sampling activities such as collecting continuous core barrel samples. Ground water at the study site occurs as an unconfined water table usually 7 feet (2.1 m) bgs. The water table at this location has been observed to fluctuate no more than 3 feet in the 8 years prior to the model prediction.

Application of this model to an FGS at a small scale would be inappropriate due to the apparent heterogeneity caused by macropores within FGS. However, if the site is conceptualized on a larger, "5 feet" or "10 feet" (well screen), scale (larger than the representative elementary volume [REV], Bear [1972]), the large volume allows for simulating the FGS as a homogeneous soil with a low effective porosity. Viewing the problem this way is important because it allows the site to fit the assumption of a homogeneous medium.

Observed LNAPL Saturation and Distribution at the Field Study Site

The exact source of the LNAPL in the subsurface is unknown but is believed to have been a surface release located relatively close (<100 feet) to the study area. LNAPL has been reported in macropores as deep as 17 feet (5.2 m) below the water table. LNAPL accumulations up to 15.3 feet (4.7 m) have been measured in observation wells prior to any LNAPL recovery. LNAPL recharge into the wells at the study site is very slow; it takes 4 to 6 months for a thickness of more than 10 feet (3 m) to accumulate. Figure 6 summarizes the LNAPL observations from a soil boring located in the study area of the field site.

LNAPL saturations in the FGS were determined in the laboratory using the Dean Stark analysis (API method RP-40) on 11 soil samples collected ~5 feet (1.5 m) above and below the water table. Eight samples had no detectable LNAPL saturation, two samples contained LNAPL at 0.1% saturation, and one sample contained LNAPL at a saturation of 1.4% (the maximum saturation observed). Certainly, the most interesting observation from this data is that a soil having maximum measured LNAPL saturations

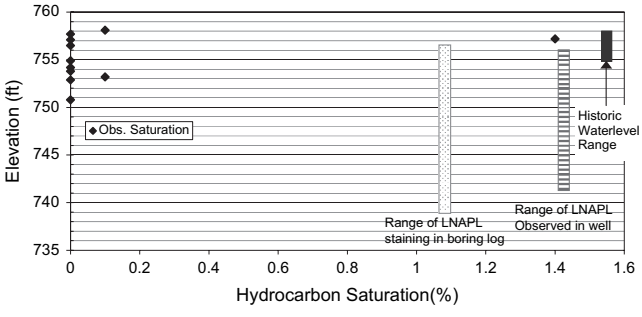

Figure 6. LNAPL condition in the boring and monitoring well at the field study site. Note the depth of LNAPL observation (staining) below the depth of water table fluctuation. Also, note the extremely low measured LNAPL saturations in the FGS from the boring. (LNAPL observations are plotted referenced to elevation, y-axis).

<2% can lead to 15.3 feet (4.7 m) of LNAPL accumulation in an observation well.

Results of Modeling

Step 1: Modeling LNAPL Distribution at the Field Study Site

The use of site-specific parameters for input into the API model was critical because many of the measured values differed significantly from literature values. Table 2 lists the soil and liquid parameters used as input in the API distribution model and also lists the literature values that would have been used in the absence of site-specific data. If literature values had been assumed for modeling at this site, the maximum predicted LNAPL saturation would have decreased from 2.7% to <0.5% and the LNAPL specific volume would have decreased from 0.09 ft^3/ft^2 (0.029 m^3/m^2) to 0.012 ft^3/ft^2 (0.004 m^3/m^2). Thus, the use of measured values for model parameters, as opposed to using estimated values derived from reference literature, may have a significant effect on the calculated LNAPL saturations (Figure 7).

Figure 7 compares the measured soil LNAPL saturations with the results of the LNAPL distribution modeling conducted at the study site. Model predictions are depicted for simulations using both assumed values from the literature and site-specific measured values. Laboratory-measured saturations are represented as diamonds in Figure 7. The maximum observed saturation was 1.4%, while the maximum model-predicted saturation was 2.7%. Overall, the model-predicted saturations matched the observed saturations remarkably well. The reason that so many (8 of 11) LNAPL saturations were reported as not detected (ND) is likely a result of scale. At the scale of the laboratory saturation analysis (1 $inch^3$) (25cc), a volume less than the REV for this system, the soil and macropore network is very heterogeneous. LNAPL-bearing macropores easily could be missed, leading to the extreme variation in observed LNAPL saturation as a likely outcome. Given the size of borehole and sampling devices, it is not possible to obtain representative soil samples for LNAPL saturation determination, regardless of the laboratory analysis method. With so many ND results, the model prediction using the literature values may appear to be a better fit to data. However, that simulation only predicted a maximum saturation of <0.5%, while 1.4% had been observed. Given the nature of the soil and scale problems, it is possible that the actual maximum saturation in place would exceed 1.4%.

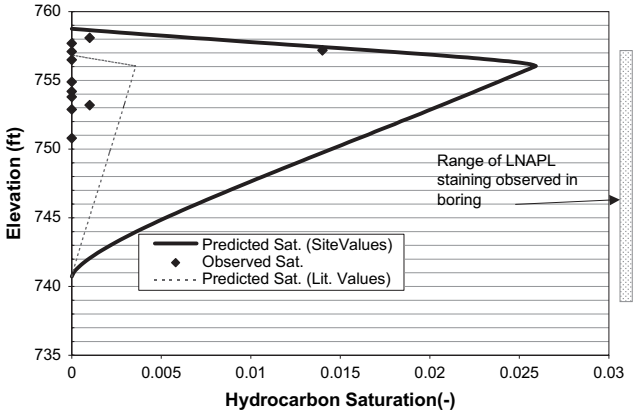

Figure 7. Comparison of observed LNAPL saturation with model-predicted saturations using both literature and site-specific soil parameters.

Most importantly, using the site-specific model parameters, the model predicted a specific LNAPL volume (D_o) of 0.09 ft^3/ft^2 (0.029 m^3/m^2) for the soil saturation profile shown in Figure 7. This calculated amount of LNAPL in the soil column is associated with an observed LNAPL thickness of 15.3 feet (4.7 m) in the observation well. The model-derived D_o is basically the summation of the area under the predicted LNAPL distribution curve shown in Figure 7 (after multiplying the saturation by the porosity).

These findings also identify a potentially significant problem of how to determine LNAPL residual saturation in FGS. The study site has considerable LNAPL accumulation in this observation well. However, the LNAPL saturations in soil samples collected from the site were significantly lower than what might be expected for a residual LNAPL saturation in an FGS. Mercer and Cohen (1990) stated "values of residual saturation in saturated media generally range from 0.15 to 0.50" and cited references for a few residual LNAPL saturations in FGS ranging from 15% to 52%. An appropriate means to determine the true residual saturation for LNAPL in FGS under field conditions needs to be developed.

Step 2: LNAPL Recovery Modeling at the Field Study Site

Recovery Model Input—field Study Site: The input parameters used in the API recovery model are listed in Table 3.

Table 2
Input Parameters for LNAPL Distribution Modeling

Parameter	Units	Site-Specific Value	Literature Value
Porosity	Ratio	0.41	
van Genuchten α	m^{-1}	0.56	0.50
van Genuchten *N*	Dimensionless	1.46	1.09
Irreducible water saturation	Ratio	0.82	
LNAPL density	g/cm^3	0.91	
Air/water surface tension	dyne/cm	65.6	72
Oil/water surface tension	dyne/cm	20.2	50
Air/oil surface tension	dyne/cm	30.7	

Note: Site-specific soil properties were obtained from an undisturbed soil sample. Site-specific fluid properties were measured from fluids collected from observation wells located within the study site. Literature values are listed if they would have been different from the site-specific value. Literature values for van Genuchten parameters are taken from Charbeneau et al. (1999) after Carsel and Parrish (1988). Literature values for surface tensions taken from Mercer and Cohen (1990).

Table 3
Parameters and the Values Used as Input for the Recovery Model

Parameter	Symbol	Value	Source	Confidence
Discharge	Q	9.36×10^4 (ft^3/d)	Initial airflows from system	Medium
Saturated screen length	L	20 (feet)	Measured	High
Relative permeability	k_{rf}	0.95 (−)	Estimated (API manual example)	Low
Density ratio	ρ_r	0.91 (−)	Lab measurement	High
Viscosity ratio	μ_{rf}	350 (−)	Lab measurement	High
Soil porosity	n	0.41 (−)	Lab measurement	High
Radius of capture	R	20 (feet)	Pilot test	Medium to low
Residual LNAPL saturation unsaturated zone	Sorv	0.2%	Estimated based on maximum observed and model values	Low
Residual LNAPL saturation saturated zone	Sors	0.8%	Estimated based on maximum observed and model values	Low
Minimum thickness: 15–10 feet	α	6.589 (feet)	Curve fit	High
Minimum thickness: 10–2.5 feet	α	2.439 (feet)	Curve fit	High
LNAPL specific yield 15–10 feet	β	0.011	Curve fit	High
LNAPL specific yield 10–2.5 feet	β	0.005	Curve fit	High

Note: Values above were used in a deterministic prediction of recovery at the study site prior to system operation.

These values were obtained from either laboratory or field measurements or were based on professional judgment. All the assumed values represent first-cut, best-estimated values and were not modified to obtain a "calibrated" best fit of the recovery data because the modeling was performed prior to recovery system operation. The modeling was intended to predict recovery prior to system operation. The source of the value and the level of confidence in the values for the model inputs are also listed in Table 3. The values listed with low confidence were obtained through combined professional experience, as any hydrogeologic model ultimately requires.

Model-Predicted LNAPL Recovery: The predicted LNAPL recovery volumes are for a total fluids extraction (TFE) system (three phases) and are dependent on observed LNAPL thickness. The API model predicts a total LNAPL recovery volume of 530 gallons (2009 L) of LNAPL in ~30 years. This is shown in Figure 8 by summing the total predicted recovery for the 15.3-foot (4.7-m) and the 10-foot (3-m) case. This summation is necessary because the LNAPL recovery is modeled as either a two- or three-stair-step discontinuous function defined by the model parameters α and β (Table 2). As a result of this approach, LNAPL recovery was modeled in two increments: the first step involved decreasing the LNAPL thickness in the observation well from 15 feet (4.7 m) to 10 feet (3 m) and the second step reduced the LNAPL from 10 feet (3 m) to 2.5 feet (0.76 m) of LNAPL thickness in the observation well. No modeling was done for the condition of LNAPL < 2.5 feet in the observation well because the LNAPL specific volume becomes so low below 2.5 feet that the recovery is essentially nil.

Figure 8 presents the model-predicted LNAPL recovery for the study site (15.3 feet) along with three other thickness scenarios (10, 5, and 3 feet). The recovery system was operating in an area where the maximum LNAPL thickness in observation wells exceeded 15 feet (4.6 m). The LNAPL at this study site was a nonvolatile weathered diesel, thus loss of mass to vapor phase is not a concern in this recovery scenario. Referring to Figure 8, to evaluate the model-predicted recovery for the study site, the 15.3-foot (4.7-m) curve is followed to its termination of 410 gallons (1553 L) recovered, with 160 gallons (606 L) lost to residual LNAPL. At that point, the LNAPL and soil conditions have been changed, as a result of the recovery efforts, to that corresponding to a 10-foot (3-m) LNAPL thickness soil condition. The 10-foot (3-m) curve is then followed to its end point at 120 gallons (455 L) recovered,

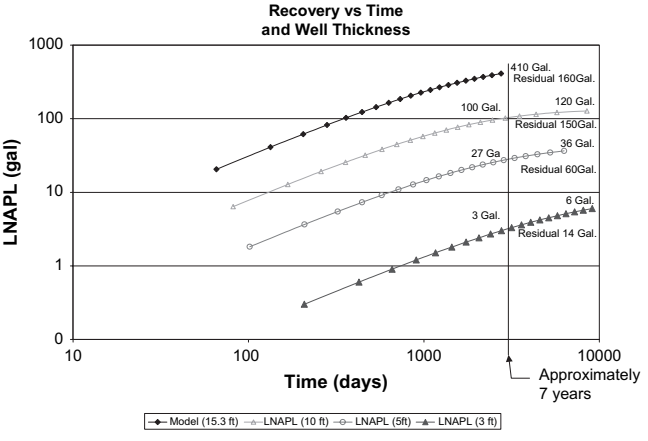

Figure 8. Predicted recovery of LNAPL from the three-phase extraction system as a function of time and initial thickness of LNAPL in a monitoring well. Model predicts 510, 100, 27, and 3 gallons of recovery in 7 years of recovery system operation in each of the 4.7-, 3-, 1.5-, and 1-m LNAPL thickness conditions (4.7- and 3-m cases are summed for total 4.7 m predicted recovery).

with 150 gallons (568 L) of LNAPL remaining as residual LNAPL. Thus, the total model-predicted recovery is the sum of 530 gallons (2009 L) recovered and 310 gallons (1174 L) left as residual in a total time of ~30 years of system operation. A new version of the Charbeneau/API model automates this stair-step analysis and eliminates the need for modeler involvement, thus making it much faster and easier to use.

Actual System LNAPL Recovery

The TFE system was in operation at the site from January 2001 through July 2002. The recovery system consisted of five 1-inch (2.54-cm) wells and one 2-inch (5.08-cm) well removing air, water, and LNAPL. The fluids were extracted with suction applied via a liquid ring pump. The system applied a vacuum of 25 to 27 inch of mercury (635 to 685 mm of Hg) to the wells. The system was operated in alternating pulse mode during the first 5 months; therefore, the actual recovery had not reached steady-state conditions with respect to water levels and flow conditions that are basic to the recovery model assumptions. In May 2001, the system was switched to full-time operation on the 2-inch (5.08-cm) well, allowing the recovery operation to reach steady-state operation. The recovery well that was used for the majority of the LNAPL recovery at the study site is constructed with 20 feet (6.1 m) of well screen located from 6 to 26 feet (1.83 to 7.92 m) bgs. All fluids were extracted from the top of the recovery well; a drop tube was not used initially. A drop tube was installed after the initial recovery became asymptotic but was not beneficial. During system operation, a well that is located 6 feet (1.83 m) from the recovery well that typically contains over 15 feet (4.57 m) of water (and/or LNAPL) was completely evacuated by the recovery system.

Figure 9 presents the model-predicted and the actual recovered LNAPL volumes for this first year and a half of recovery system operation. The actual LNAPL recovery line appears stair stepped as a result of the way the project accounts for LNAPL recovery. The LNAPL is recorded as recovered on the day that the holding tank is emptied. Thus, the large increase in recovery shown on July 12, 2001, is actually all the LNAPL recovered by the system from June through July 12. Through May 15, 2002, the

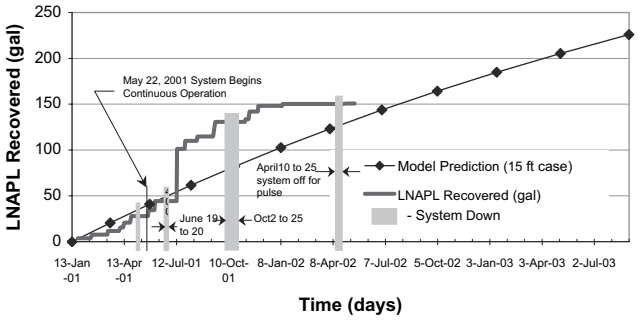

Figure 9. Comparison of predicted vs. actual LNAPL recovery using the three-phase system at the field study site.

model predicted the recovery of 133 gallons (504 L) of the weathered diesel, while the system had recovered an actual 151 gallons (572 L). The actual volume of LNAPL recovered is ~14% above the model prediction. Considering the possible variability of many of the model input parameters (radius of capture, average LNAPL thickness in the radius of capture, system discharge rate, etc.), the model has predicted the actual recovery very well. One should also recall that this modeling simulation has not been calibrated to fit the actual recovered volume and that the prediction is based on estimates made prior to system startup.

Because no LNAPL was recovered by the system for 6 months, the system was shut off on July 19, 2002. The system remained off for 5 months through December 2002. Table 4 provides measurements of LNAPL thickness in wells near the extraction well before system startup and 1 week and 5 months after system shut-down. From the data contained in Table 4, it appears that the system has been effective in recovering the LNAPL that had been contained within a radius of 15 feet (4.6 m) to 20 feet (6.1 m) of the extraction well. Also note that, due to a lack of precipitation, the water table at the site, outside the influence of the system, has dropped ~2.5 feet (0.76 m) over the period from January 2001 to December 2002. Therefore, the decrease in LNAPL thickness can be assumed as the result of recovery efforts and not the result of water table rise.

The aforementioned recovery information requires the discussion of the difference between model-predicted and actual recovered LNAPL volumes. The model predicted a total recoverable LNAPL volume of 530 gallons (2009 L).

Table 4
Observation Well LNAPL Thickness in Observation Wells Near the Extraction Well

Well	Distance from Extraction Well (feet)	Initial Thickness (feet)	Shutoff Thickness (feet) (1 week)	Rebounded Thickness (feet) (5 months)
MW-78A	5.7	0.3	0.1	0.8
SC-15	11.7	15.3	0.2	0.9
SC-25	16.0	9.9	0.6	2.0
SC-24	20.9	14.6	3.9	7.9
SC-14	31.2	2.4	0.8	3.3

Note: Shutoff thickness is that observed in the well 1 week after the recovery system was shut off. Rebounded thickness is that observed in the well 5 months after recovery system was shut off.

This was based on an assumed worst-case LNAPL soil condition represented by 15.3 feet (4.7 m) of LNAPL in all wells throughout the estimated 20-foot (6.1-m) radius of capture for the system. The estimate was also based on running the system for 30 years. The LNAPL thickness within the model radius around the extraction well at the time of system startup ranged from 0.55 feet (0.17 m) to 15.3 feet (4.7 m). Thus, by assuming 15.3 feet (4.7 m), the model was bound to overpredict the total recoverable LNAPL volume.

The cost of installation, maintenance, and operation of this system for the year and a half of operation was ~$175,000. During operation, this system recovered 151 gallons of weathered diesel, a ratio of $1158 per gallon (260 €/L) of LNAPL. Note that this recovery was conducted in the area of the site with the most extensive LNAPL impact. Operation of recovery systems in other areas of this site with <5 feet (1.5 m) of LNAPL in wells would likely result in much poorer recoveries and economics.

Consideration of Vertical Gradient: Impact on LNAPL Distribution and Recovery Modeling

The aforementioned distribution and recovery modeling was conducted prior to recovery system startup and was completed in a deterministic fashion using the models available at that time. At that time, it was understood that the hydraulic gradient in the FGS at the study site contained a strong downward vertical component. It was suspected that this vertical gradient could have a significant impact on the predicted LNAPL distribution and recovery. However, the API model did not allow for assessment of the impact of vertical gradient.

As a result of peer review comments received on the initial draft of this paper, the occurrence and magnitude of the vertical gradient was investigated. In addition, a proprietary, draft version of the API model was made available (R. Charbeneau, personal communication, 2003), which incorporates vertical gradient. The resulting reevaluation of the model-predicted LNAPL distribution and recovery is discussed subsequently.

Hydraulic Gradient at the Test Site

Vertical hydraulic gradient data for the test site were obtained from a well pair located ~200 feet (61 m) from the well used by the LNAPL recovery system. Thirty-seven measurements of the vertical hydraulic gradient were collected in the time period from December 1986 to March 2003. These data ranged from 0.37 downward to 0.05 upward, with a time-weighted average value of 0.05 downward. The large range in gradient readings appears to be the result of recent precipitation events or lack thereof.

Revised LNAPL Distribution and Recovery Modeling

A revised draft version of the API model that accounts for the pressure effect of a vertical hydraulic gradient was used to predict the LNAPL distribution and recovery. This revision to the model accounts for a vertical hydraulic gradient by introducing a modified capillary scaling factor that incorporates the effects of the vertical gradient on the local capillary pressure. Using this revised model, the predicted LNAPL distribution at the study site is depicted in Figure 10. Comparison of predicted LNAPL saturations from the hydrostatic case (Figure 7) and the downward vertical gradient case (Figure 10) shows that the downward vertical gradient significantly decreases the maximum predicted saturation from 2.7% to 1%. This result is reasonable because the vertical gradient essentially lowers the capillary pressure, thus lowering the LNAPL saturation. Accordingly, the model-predicted recoverable LNAPL volume decreases in the case with the vertical gradient to 290 gallons (1099 L) from the 530 gallons (2009 L) in the hydrostatic model prediction. Although this revised model slightly underpredicts the maximum LNAPL saturation that was observed (1.4% observed vs. 1% predicted), the model-predicted recovery of 290 gallons (1099 L) is closer to the observed system recovery of 151 gallons (572 L).

Conclusion

A revised conceptual model for the behavior of LNAPL in FGS has been presented that builds on previous work pertaining to DNAPL migration in FGS and that of Lenhard and Parker (1990) and Farr et al. (1990). This conceptualization explains how LNAPL can penetrate below the water table, even in the absence of water table fluctuation. As a result of LNAPL presence below the water table, large LNAPL accumulations in observation wells can more easily be explained. The calculations and fieldwork presented here indicate that macropores control the saturation, distribution, and mobility of LNAPL in FGS. Through soil sampling and the determination of site-specific hydrogeology, moisture retention and fluid properties, it is possible, using the Charbeneau/API model, to predict the equilibrium LNAPL saturation in an FGS profile. In addition, this model allows the ability to predict LNAPL recovery from FGS much more accurately than previously believed possible.

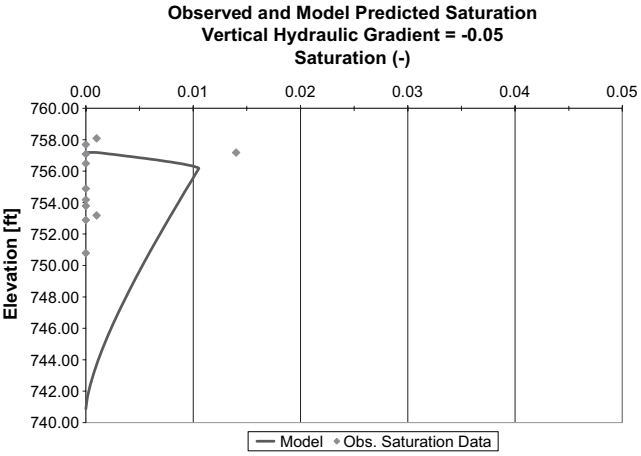

Figure 10. Comparison of observed LNAPL saturation with revised model-predicted saturations accounting for site measured vertical hydraulic gradient (using same model parameters as hydrostatic model–Table 2).

Acknowledgments

The authors would like to thank the peer reviewers of this paper from Ground Water Monitoring and Remediation, Dr. Randall Charbeneau, Dr. Jack Parker, and a third reviewer, for their obvious effort in reviewing and providing extremely beneficial comments. The authors would like to thank the following individuals for their work at the study sites: Jean Lawlor, Chris Robb, Jerry Hammer, and Lew Ditto. The authors appreciate the technical support from the following individuals: Stephanie Fiorenza, Lloyd Dunlap, Len Crame, Michael Hagood, Michael Whelan, Kevin Heaton, Paul Furtick, C.C. Rice, Cindy Collier, Roberta Saielli, and Michael Brady of PTS Laboratories. The authors appreciate the financial support from BP projects managed by many of those listed above . Mark would especially like to dedicate his work to Dr. Patrick Domenico, a wonderful teacher, mentor, and friend.

Editor's Note: The use of brand names in peer-reviewed papers is for identification purposes only and does not constitute endorsement by the authors, their employers, or the National Ground Water Association.

References

Ballestero, T.P., F.R. Fiedler, and N.E. Kinner. 1994. An investigation of the relationship between actual and apparent gasoline thickness in a uniform sand aquifer. *Ground Water* 32, no. 5: 708–718.

Bear, J. 1972. *Dynamics of Fluids in Porous Media*. Elsevier Publishing. New York, NY

Bianchi, W.C., and E.E. Haskell Jr. 1966. Air in the vadose zone as it affects water movements beneath a recharge basin. *Water Resources Research* 2, no. 2: 315–322.

Brockman, S.C., and J.P. Szabo. 2000. Fractures and their distribution in the tills of Ohio. *Ohio Journal of Science* 100, no. 3/4: 39–55.

Brooks, R.H., and A.T. Corey. 1964. Hydraulic properties of porous media, Hydrology Paper 3. Fort Collins, Colorado: Colorado State University.

Charbeneau, R.J. 2004. Beta version of model incorporating effect of vertical gradient. Personal communication.

Charbeneau, R.J. 2005. Simple models for the design of free-product recovery systems for petroleum hydrocarbon liquid. Submitted to Ground Water Monitoring and Remediation.

Charbeneau, R.J., and C.Y. *Chiang*. 1995. Estimation of free-hydrocarbon recovery from dual-pump systems. *Ground Water* 33, no. 4: 627–634.

Charbeneau, R.J., R.T. Johns, L.W. Lake, and M.J. McAdams. 1999. Free-product recovery of petroleum hydrocarbon liquids. API publication 4682. API Publications, Washington, DC.

Corey, A.T. 1986. Mechanics of immiscible fluids in porous media. Water Resources Publication. Littleton, CO.

Domenico, P.A., and F.W. Schwartz. 1990. *Physical and Chemical Hydrogeology.* Wiley & Sons. New York, NY.

Farr, A.M., R.J. Houghtalen, and D.B. McWhorter. 1990. Volume estimation of light nonaqueous phase liquids in porous media.- *Ground Water* 28, no. 1: 48.

Freeze, A.R., and D.B. McWhorter. 1997. A framework for assessing risk reduction due to DNAPL mass removal from low-permeability soils. *Ground Water* 35, no. 1: 111–123.

Freeze, A.R., and P.A. Witherspoon. 1967. Theoretical analysis of regional ground-water flow. II. Effect of water table configuration and subsurface permeability variations. *Water Resources Research* 22, no. 13: 623–634.

Hinsby, K., L.D. McKay, P. Jorgensen, M. Lenczewski, and C.P. Gerba. 1996. Fracture aperture measurements and migration of solutes, viruses, and immiscible creosote in a column of clay-rich till. *Ground Water* 34, no. 6: 1065.

Huntley, D., J.W. Wallace, and R.N. Hawk. 1994. Nonaqueous phase hydrocarbon in a fine-grained sandstone: 2. Effect of local sediment variability on the estimation of hydrocarbon volumes. *Ground Water* 32, no. 5: 778–783.

Jury, W.A., W.R. Gardner, and W.H. Gardner. 1991. *Soil Physics*. Wiley and Sons. New York, NY.

Kramer, W.H. 1982. Ground-water pollution from gasoline. *Ground Water Monitoring and Review* 2, no. 2: 18–22.

Kueper, B.H., and D.B. McWhorter. 1991. The behavior of dense, nonaqueous phase liquids in fractured clay and rock. *Ground Water* 29, no. 5: 716–728.

Lenhard, R.J., and J.C. Parker. 1990. Estimation of free hydrocarbon volume from fluid levels in monitoring wells.*Ground Water* 28, no. 1: 57.

McWhorter, D. 1995. Relevant processes concerning hydrocarbon contamination in low permeability soils: Petroleum contaminated low permeability soil. API Publishing 4631. API Publishing. Washington, DC.

McWhorter, D.B. 1971. Infiltration affected by flow of air. Hydrology Papers 49. Fort Collins, Colorado: Colorado State University.

Mercer, J.W., and R.M. Cohen. 1990. A review of immiscible fluids in the subsurface: Properties, models, characterization and remediation. *Journal of Contaminant Hydrology* 6, no. 6: 107–163.

O'Hara, S.K., B.L. Parker, P.R. Jorgensen, and J.A. Cherry. 2000. Trichloroethene DNAPL flow and mass distribution in naturally fractured clay: Evidence of aperture variability. *Water Resources Research* 36, no. 1: 135–147.

Parker, B.L., R.W. Gillham, and J.A. Cherry. 1994. Diffusive disappearance of immiscible-phase organic liquids in fractured geologic media. *Ground Water* 32, no. 5: 805–820.

PTS Laboratories. 2002. BP Project report. PTS file 31548. Santa fe springs, CA

PTS Laboratories. 2000. BP Project report. PTS file 30367. Santa fe springs, CA

Simpkins, W.W., and K.R. Bradbury. 1992. Groundwater flow, velocity, and age in a thick, fine-grained till unit in Southeastern Wisconsin. *Journal of Hydrology* 132, no. 132: 283–319.

Stephens, D.B. 1996. *Vadose Zone Hydrology.* Lewis Publishers, Boca Raton, FL

van Dam, J. 1967. The migration of hydrocarbons in a water-bearing stratum. In *The Joint Problems of the Oil and Water Industries: The Institute of Petroleum Symposium*, ed. P. Hepple, 55–96. Brighton, London. January 18–20.

van Genuchten, M.T. 1980. A closed-form equation for predicting the hydraulic conductivity of unsaturated soil. *Soil Sci. Soc. Am. J*. 44, 892–898.

Zilliox, L., and P. Muntzer. 1975. Effects of hydrodynamic processes on the development of ground-water pollution: Study on physical models in a saturated porous media. *Progress in Water Technology* 7, no. 3/4: 561–568.

Biographical Sketches

Mark Adamski *PG, is an environmental engineer/geologist with BP-Remediation Management p.l.c. (a BP affiliated company). He has spent his 11-year-BP career remediating hydrocarbon-contaminated sites as well as modeling fluid flow for both*

environmental and petroleum exploration projects. His environmental experience has been focused on chemical and refining facilities. He has a B.S. in geological engineering from the University of Arizona and a M.S. in Hydrogeology from Texas A&M University. He may be reached at BP-Remediation Management p.l.c., 501 Westlake Park Boulevard, Houston, TX 77079.

***Victor Kremesec** Ph.D, has more than 13 years experience in remediating hydrocarbon-contaminated sites for BP-Remediation Management p.l.c. (a BP affiliated company). He is a member of the Advisory Committee for the API Soils/Groundwater Technical Task Force and a member of the Technical Advisory Committee of the Florida DEP. He has a Ph.D. in chemical engineering from Northwestern University. He may be reached at BP-Remediation Management p.l.c., 28100 Torch Parkway, Warrenville, IL 60555.*

***Ravi Kolhatkar** Ph.D, is an environmental engineer with BP-Remediation Management p.l.c. (a BP affiliated company). He is an active member of the API Soil and Groundwater Technical Task Force and has been working on MTBE remediation, LNAPL recovery, and natural attenuation issues for more than 4 years. He has a Ph.D. in chemical engineering from the University of Tulsa, Oklahoma. He may be reached at BP-Remediation Management p.l.c., 6 Centerpointe Drive, La Palma, CA 90623.*

***Chris Pearson** P.E., is with GeoWest Golden Inc.,/TriTechnics/ThermoRetec Corporation, Golden, Colorado, from 1992 to present. He has a B.S. in civil engineering from the University of California at Berkeley and an M.S. in groundwater engineering from Colorado State University, Colorado. Chris has more than 10 years experience as an environmental engineer working at multiple petroleum refineries and exploration and production sites in North Dakota, Missouri, Colorado, Wyoming, and Utah. He may be reached at Retec, 1726 Cole Boulevard, Building 22, Suite 150, Golden, CO 80401.*

***M. Elizabeth Rowan** P.G., C.G.W.P., is with RMT Inc. (1993 to present), previously with Sirrine Environmental (now EarthTech), Dames and Moore, and regulatory agencies in Washington and Nebraska. She has a B.S. in environmental studies from the University of Tennessee at Chattanooga and an M.S. in geology from the University of Nebraska, Lincoln. She is a Registered Geologist in South Carolina, Georgia, Alabama, Tennessee, and Missouri. She is also a Certified Ground Water Professional (National Ground Water Association). She has almost 18 years experience in the environmental field with both regulatory agencies and the private sector. She may be reached at RMT, 53 Century Boulevard, Suite 150, Nashville, TN 37214.*